Localization in a random magnetic field: The semiclassical limit

D. K. K. Lee
Department of Physics, Massachusetts Institute of Technology, 77 Massachusetts Avenue, Cambridge, Massachusetts 02139

J. T. Chalker and D. Y. K. Ko
Theoretical Physics, University of Oxford, 1 Keble Road, Oxford, OX1 3NP, United Kingdom
(Received 7 April 1994)

We study the two-dimensional electron gas in the presence of a random perpendicular magnetic field. We examine, in particular, the limit in which the correlation length of the random field is large compared to the typical magnetic length. In this limit, a semiclassical approach can be used to understand a large part of the energy spectrum. To investigate localization, we introduce a simplified model, in which electrons propagate coherently on a random network derived from the classical trajectories. The same network model (with different parameters) also represents electron motion in a *uniform* magnetic field and a random *scalar* potential, in a spin-degenerate Landau level. Requiring that the global phase diagram of our model be consistent with Khmelnitskii's scaling flow for the quantum Hall effect, we argue that all electron states in a random magnetic field are localized in the semiclassical limit. We present the results of numerical simulations of the model in support of this conclusion.

I. INTRODUCTION

There has been much recent interest in the quantum mechanics of a charged particle in a random vector potential.[1–6] This problem arises both within gauge theories of doped Mott insulators,[7,8] and in the Chern-Simons mean-field theory of a half-filled Landau level.[9,10] It also deserves attention as a counterpart to the much-studied case of motion in a random scalar potential. In this paper we consider the two-dimensional electron gas in the presence of a random perpendicular magnetic field, taking a semiclassical limit in which the spatial variation of the random magnetic field is smooth compared to the typical magnetic length. We develop a simplified description of the system in terms of a generalization of the random network model, introduced previously by one of us[11] in the context of the integer quantum Hall effect.

The generalized network model also serves, with different parameters, as a representation of a spin-degenerate Landau level, and by studying its global phase diagram we gain insight into both problems. Most importantly, we argue that the Khmelnitskii-Pruisken scaling theory[12,13] for the quantum Hall effect carries the implication that all states in a smoothly varying random magnetic field should be localized. This conclusion is supported by the results of extensive numerical simulations of our generalized network model. In addition, these simulations provide information on the delocalization transition in spin-degenerate Landau levels, which leads us to propose an additional interpretation for recent experiments[14–18] that measure the associated critical exponents.

Our treatment of the semiclassical limit, reached when the correlation length for the magnetic field is large, is complementary to earlier work, which has been concerned with field distributions having a short or vanishing correlation length. In particular, we use the term *semiclassical* in a different sense from Altshuler and Ioffe,[19] and Khveshchenko and Meshkov,[20] who introduced an eikonal approximation appropriate for fast particles.

While some quantities of interest, most notably the density of states in energy, are clearly model dependent, it is reasonable to expect a generic answer to the question: are eigenstates localized in a random magnetic field? Within the established framework of localization theory, the natural assumption is that, in two dimensions, they are, no matter how large the conductivity at short distances. Specifically, the system should belong to the unitary universality class, since time-reversal symmetry is broken and the average Hall conductivity is zero. Nevertheless, conflicting conclusions have been reached from numerical simulations of tight-binding models with a random vector potential introduced via the phases of hopping matrix elements. Some authors[3,10] have suggested that there exists a range of energies for which the states are not exponentially localized, and it has been conjectures[5,6] that long-range correlations in random gauge fields might result in an additional universality class. We find that this is not the case, although the arguments that place our model in the unitary class are less straightforward than one might expect, and involve a detailed discussion of boundary conditions.

The remainder of this paper is arranged as follows. In Sec. II, we develop the adiabatic description of electron motion in the semiclassical limit. This provides us with a framework in which to calculate the density of states over a large range of energies. In Sec. III, we discuss both classical and quantum scattering of low-energy electrons near saddle points of the magnetic field. This leads us to a random network model, in which the links of the network represent electron trajectories associated with contours of zero magnetic field, and the nodes represent the saddle points. We proceed, in Sec. IV, to discuss the

0163-1829/94/50(8)/5272(14)/$06.00

phase diagram of this network model, using scaling ideas and numerical simulations. Our results are summarized in Sec. V. A brief account of our main conclusions has been presented elsewhere.[21]

II. THE SEMICLASSICAL LIMIT

A. An adiabatic picture

In this section, we review the adiabatic theory for the classical and quantum motion of a charged particle in a magnetic field that varies smoothly in space.[22,23] The approach has close analogs with the application to the quantum Hall effect of semiclassical theory for motion in a scalar random potential under a uniform magnetic field.[24–28] Denoting the correlation length of the random magnetic field by λ and the variance by $\langle B(\mathbf{r})^2\rangle = B_0^2$, our semiclassical limit is defined as the regime in which the cyclotron radius in a field B_0, $l_0=(\hbar/eB_0)^{1/2}$, satisfies $l_0 \ll \lambda$. Under these conditions, one can separate the motion into two components: a rapid cyclotron orbit and slow drift of the guiding center. We develop a semiclassical picture for the eigenstates in which wave functions are concentrated near a given contour of the magnetic field. This allows us to discuss the density of states over a large range of energies. We defer to Sec. III a treatment of the scattering at saddle points of the field strength, which is necessary for understanding localization in this system.

Consider first the classical motion in a constant field gradient. As described by Müller,[29] there are two types of classical trajectories. These are illustrated in Fig. 1. Where the magnetic field is large, the particle follows cyclotron orbits whose guiding center drifts along contours of constant field. Where the magnetic field is small, there exist snakelike trajectories which cross the $B=0$ line. These trajectories have a mean velocity in the *opposite* direction to the cyclotron drift. In the context of localization in a random field distributed symmetrically about zero, it is the snake trajectories that are of greatest interest, because extended states, if any exist, will be associated with the percolation of the $B=0$ contour. Writing the magnetic field $(0,0,B_z)$ as

$$B_z(x,y) = -B_0 b y/\lambda \ , \tag{1}$$

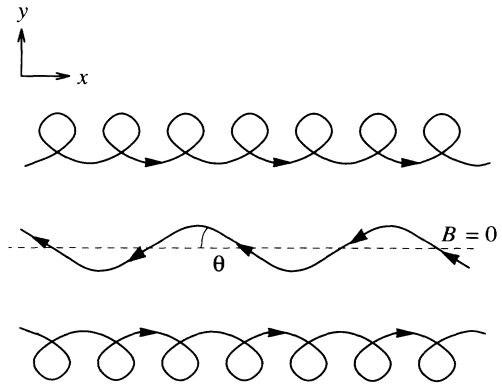

FIG. 1. Classical trajectories in a magnetic-field gradient.

the equation of motion, $m\ddot{\mathbf{r}} = e\dot{\mathbf{r}}\times\mathbf{B}$ can be cast in the form

$$\frac{1}{v_0}\frac{dx}{dt} = -\cos\theta - \frac{b}{2\epsilon}\left[\frac{y}{\lambda}\right]^2 ,$$
$$\frac{1}{v_0}\frac{dy}{dt} = [\sin^2\theta - V(y)]^{1/2} , \tag{2}$$

with

$$V(y) = \frac{b}{\epsilon}\left[\frac{y}{\lambda}\right]^2\left[\frac{b}{4\epsilon}\left[\frac{y}{\lambda}\right]^2 + \cos\theta\right] ,$$

where v_0 is the speed of the particle and θ is the angle at which the trajectory cuts the $B=0$ contour (see Fig. 1 for $b>0$). The ratio of the typical cyclotron radius to the correlation length, $\epsilon = mv_0/eB_0\lambda$, is a small parameter for a smooth field configuration.

Translational symmetry ensures that $\cos\theta$ is a constant of the longitudinal motion.[30] The transverse motion can be interpreted as oscillation in a potential well, $V(y)$, whose size and shape depend on the field gradient and the longitudinal velocity of the particle.

There are strong similarities between the classical motion and the quantum dynamics in the semiclassical limit in which field variations are smooth, and the typical magnetic length l_0 is small compared with λ. In the Landau gauge $B_z = -\partial A_x/\partial y$, the wave function can be factorized as $\psi(x,y) = e^{ikx}\phi(y)$, where the wave vector k is the conserved quantity analogous to $-v_0\cos\theta$ in the classical description above. The Schrödinger equation for the transverse motion represented by $\phi(y)$ is

$$\frac{1}{2}\left[-\Lambda^2\frac{d^2}{dy^2} + \left[k\Lambda - \frac{y^2}{2\Lambda^2}\right]^2\right]\phi = \frac{E_n(k)}{E_\Lambda}\phi \ , \tag{3}$$

where $\Lambda = (\hbar/e|\nabla B|)^{1/3}$ and $E_\Lambda = \hbar/m\Lambda^2$ are the natural length and energy scales of the problem. The energy spectrum $E_n(k)/E_\Lambda$ is shown in Fig. 2.

For large and positive $k\Lambda$, the particle is laterally confined to either side of a double-well potential by a barrier of height $\frac{1}{2}(k\Lambda)^2 E_\Lambda$ centered on the $B=0$ line. The

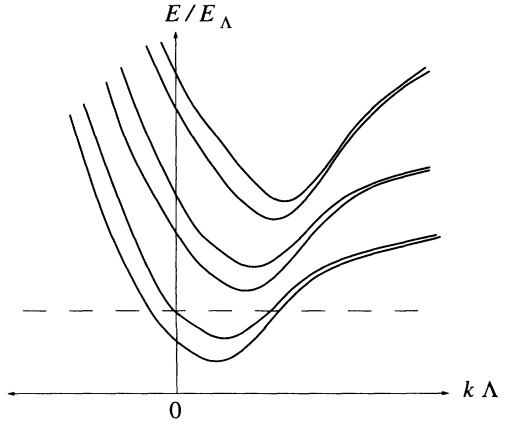

FIG. 2. Dispersion relation for particle in a constant magnetic-field gradient. Dotted line indicates an energy at which a pair of snake states is found.

eigenstates below this barrier are "local Landau levels" and correspond to classical cyclotron drift on a finite-B contour at $y=\pm y_k=\pm(2k\Lambda^3)^{1/2}$. These states carry probability current in the positive-x direction. Neglecting tunnel splitting, their energy is

$$E_n=(n+\tfrac{1}{2})\frac{e\hbar}{m}|B(y_k)| . \tag{4}$$

For large and negative $k\Lambda$, the confining potential is a single well centered at $y=0$. The eigenstates correspond to the snake trajectories and carry probability current in the negative-x direction.[29]

Between these two branches of opposite velocities, the energy spectrum $E_n(k)$ must have a minimum. Behavior near the minimum is of interest because of the associated singularity in the local density of states. One can see from the Schrödinger equation satisfied by $\phi(y)$ [Eq. (3)] that this occurs at positive k, when the description in terms of local Landau levels breaks down and tunneling between the two sides of the double well becomes significant. In this intermediate regime, the wave function has significant amplitude near the line on which $B=0$. To identify the value of k at which this occurs, we compare the lateral extent of the wave function, $\phi(y)$, within one of the wells of the potential, with the distance between the bottom of a well and the top of the central barrier. The lateral extent is given by $(2n+1)^{1/2}l(B(y_k))$, where $l(B)=(\hbar/eB)^{1/2}$ is the local magnetic length. Comparing this with the position of the center of the state, $y=y_k$, we find that tunneling is significant when

$$k\Lambda\sim(n+\tfrac{1}{2})^{2/3} . \tag{5}$$

We shall take the solutions of this translationally invariant problem as asymptotic scattering states in a simplified model (the network model) which we use to study localization. In this context, it is useful to note from Fig. 2 that, unless an energy is chosen especially to lie close to a minimum of a band, the negative-k states, called "snake states" by Chklovskii and Lee[31] (and also the local Landau states at positive k), occur in *pairs* at a given energy. This leads us to consider network models with an even number of channels on each link of the network, in contrast to the original single-channel network for the spin-split Landau level.[11] In the simplest case, one restricts attention to just two snake states. A model in which these are the only states (over a certain energy range) has been proposed in Ref. 31, taking the field to switch abruptly between two values, $\pm B_0$, as the contour is crossed. There exist only two states at energies lying between those of the lowest two Landau levels in a uniform field of strength B_0, as illustrated in Fig. 3.

Having discussed motion in a translationally invariant field gradient, let us consider next the effect of a slowly changing magnetic gradient, for which $b=b(x/\lambda)$. The motion, in particular the guiding-center drift along finite-B contours, is analogous to adiabatic motion in a strong uniform field with a smooth scalar potential,[24–28] in which guiding centers drift along equipotentials. We focus on the behavior of the snake trajectories in the following discussion.

In classical motion (2), the angle θ is no longer a constant. It remains, however, a useful quantity if ϵ is small, so that the variations in the magnetic field are sufficiently smooth. More specifically, one finds from Eq. (2) that the distance traveled along the contour in one period of the lateral oscillations varies as $(\epsilon/b)^{1/2}\lambda$, and hence that the change in the field gradient in one cycle is small in the limit $\epsilon\to 0$. In this limit one can solve the equation of motion for y by treating the field gradient b as a parameter which varies slowly in time. According to the Hamilton-Jacobi theory, the action variable for these oscillations $I=\oint m\dot{y}\,dy$ is an approximate invariant. One may use this adiabatic invariance to follow the evolution of the snake trajectory along the zero-field contour (see the Appendix).

There is an analogous adiabatic theory for the quantum motion. One may track the wave vector k of a snake state as a function of position along the zero-field contour. In this context, adiabaticity means that the level index n remains an approximate quantum number.

More generally, one can construct eigenenergy surfaces, labeled by the quantum number n, in the three-dimensional space described by the coordinates $(\mathbf{r},E)$. Each surface traces out the positions of peaks in the local density of states $\rho(\mathbf{r},E;n)$ for a given n, and has branches of two kinds. The first kind exists in regions where the magnetic field is large enough that Landau levels can be defined locally, so that the eigenenergy surfaces are well approximated by $E=(n+1/2)\hbar e|B(\mathbf{r})|/m$. The second kind of surface, corresponding to the snake states, follows the $B=0$ contours and is parallel to the E axis. These two kinds of surfaces do not intersect the $E=0$ plane at $B(\mathbf{r})=0$. Instead, the surfaces have minima in energy near $B=0$ contours, corresponding to eigenstates of zero group velocity, as discussed above (see Fig. 2). The simplification that arises in the adiabatic limit of the quantum problem is the suppression of hybridization between states on surfaces of different n.

Let us illustrate the behavior in the adiabatic limit by considering a specific field configuration which is a form

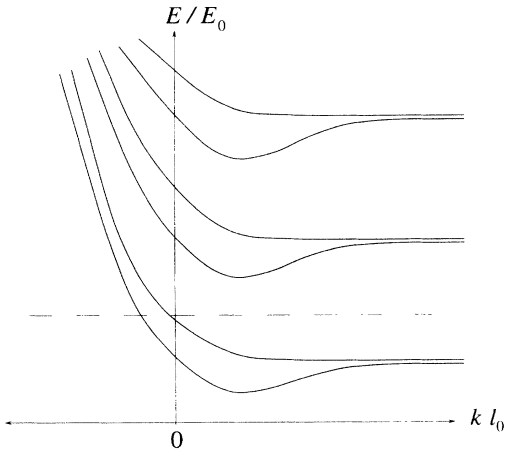

FIG. 3. Dispersion relation for a particle in a discontinuous field configuration: $B(y)=B_0\mathrm{sgn}y$. Dotted line indicates an energy at which a pair of snake states is found.

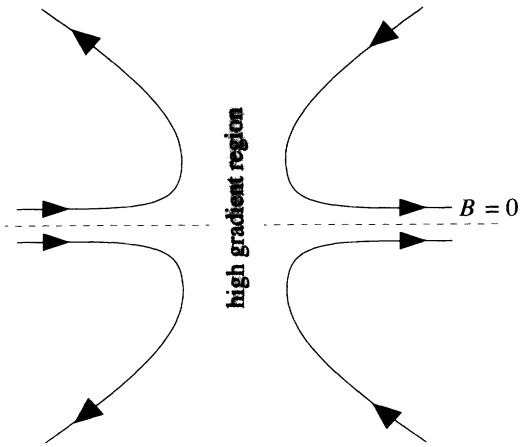

FIG. 4. Schematic illustration of the reflection from snake states onto finite-field contours at a magnetic bottleneck.

of magnetic bottleneck: we take $|\nabla B|$ to increase with distance along a $B=0$ contour. Classically, this has the consequence that a snake trajectory is reflected by the rising field gradient onto a trajectory on a nearby finite-B contour (and vice versa). A schematic illustration of this is given in Fig. 4. In the quantum problem, the rising gradient causes the minimum energy of a given band with index $n=n_0$, which varies as $E_{\text{slope}} \propto |\nabla B|^{2/3}$, to approach E from below. This means that the two wave vectors $k_{\alpha,\beta}(n_0)$ associated with the two branches of opposite group velocities on the eigenenergy surface n_0 approach each other as the magnetic gradient increases. A strong admixture of these k states must occur near the classical turning point. In the adiabatic limit $\lambda \to \infty$, the mixing occurs only between the states $k_{\alpha,\beta}(n_0)$, and hybridization with states on other energy surfaces ($n < n_0$) is weak.

In summary, we have argued that motion in a smooth random magnetic field is semiclassical in the sense that the quantum wave functions have close analogs with classical trajectories, including those found in the neighborhood of $B=0$ lines. An adiabatic picture has been developed for the quantum motion by treating the system locally using our understanding of motion along straight, parallel magnetic-field contours (3).

B. Density of states in the semiclassical limit

We now discuss the density of states in the semiclassical limit, introduced above. There are several relevant energy and length scales. The largest pair are the typical cyclotron energy $E_0=eB_0/m$ and the associated magnetic length l_0. In addition, the typical gradient of the magnetic field defines a length scale $l_{\text{slope}}=\Lambda(\nabla B=B_0/\lambda)=(l_0^2\lambda)^{1/3}$, and an energy scale $E_{\text{slope}}=E_\Lambda=E_0(l_0/\lambda)^{2/3} \ll E_0$ for the states near zero-field contours. There is also an even smaller scale, $E_{\text{saddle}}=(l_0/\lambda)E_0$, associated with states near a saddle point, typified by $B(x,y)=B_0xy/\lambda^2$.

For the bulk of the spectrum, the density of states is dominated by contributions from local Landau levels on the finite-B contours. The low-energy limit to the regime of applicability of the local-Landau-level description has been discussed in Sec. II A in the special case of a constant magnetic-field gradient [see Eq. (5)]. The result can be expressed in terms of energy as

$$E/E_0 \gg (2n+1)^{4/3}(l_0/\lambda)^{2/3} . \tag{6}$$

Details are presented in the Appendix.

There is also a high-energy limit to the regime in which the local-Landau-level picture applies. It is necessary that the lateral extent of the wave function, $(2n+1)^{1/2}l(B)$, should be small compared to the correlation length λ. Taking the typical field gradient to be B_0/λ and using (4), we find the condition

$$E/E_0 \ll (B/B_0)^2(\lambda/l_0)^2 . \tag{7}$$

In other words, as $\lambda/l_0 \to \infty$, the local-Landau-level picture is applicable in the energy range

$$(\lambda/l_0)^2 \gg E/E_0 \gg (l_0/\lambda)^{2/3} , \tag{8}$$

except for the snake states on the $B=0$ lines and the finite-B states with $n > n_{\max} \simeq (E/E_{\text{slope}})^{3/4}$. Taking the probability distribution of the field strength at a point to be $B_0^{-1}P(B/B_0)$, the contribution of the local Landau levels to the density of states is

$$\rho_{\text{bulk}}(E) \simeq \int_{-\infty}^{\infty} \frac{dB}{B_0} \sum_{n=0}^{n_{\max}} \frac{1}{2\pi l(B)^2} \delta[E-E_n(B)]P(B/B_0)$$
$$= \frac{2mE}{\pi\hbar^2 E_0} \sum_{n=0}^{n_{\max}} \frac{1}{(2n+1)^2} \left[P\left[\frac{2E}{(2n+1)E_0} \right] + P\left[\frac{2E}{(2n+1)E_0} \right] \right] , \tag{9}$$

where $l(B)$ and $E_n(B)$ are the local cyclotron length and energies, respectively. We have ignored snake states, which are also present in this energy range: their contribution to the density of states is small because they occupy only a small fraction of the system area.

At energies above the range (8), wave functions spread out over many correlation lengths, and the physics should be similar to that of a particle in a white-noise magnetic field. In this case, the density of states approaches the zero-field value.[20] Let us focus instead on the low-energy part of the spectrum. At energies below the range (8), the leading contribution to the density of states comes from the states of low group velocity near minima in the dispersion relation of Fig. 2. We use the WKB approximation (outlined in the Appendix) to estimate the resulting contribution to the low-energy density of states. The quasi-one-dimensional motion of these states means that the contribution of each band to

the density of states has an inverse square-root singularity. Let the probability distribution for each component of the field gradient $B'=(\nabla B)_{x,y}$ be given by $(\lambda/B_0)\tilde{P}(\lambda B'/B_0)$. The contribution per unit length of $B=0$ contour to the density of states is

$$\rho_{\text{line}}(E)\simeq\frac{ml_{\text{slope}}}{\hbar^2 a'}\sum_{n=0}^{\infty}\int_0^{E/E_{\text{slope}}}\frac{\omega^{1/2}}{(2n+1)^2(E/E_{\text{slope}}-\omega)^{1/2}}[\tilde{P}(\omega_n^{3/2})+\tilde{P}(-\omega_n^{3/2}]d\omega\ , \tag{10}$$

with $\omega_n=(2n+1)^{-4/3}\omega/a$, where a and a' are constants of the order of unity. Thus, assuming that $\tilde{P}(0)$ is finite, the contribution to the density of states per unit area is

$$\rho_{\text{line}}/\lambda\sim(l_0/\lambda)^{2/3}E/E_{\text{slope}}\ . \tag{11}$$

Note that the square-root divergences of each band have been smoothed out in the averaging. The energy dependence of the density of states at low energies is the same as in Eq. (9): [$\rho_{\text{bulk}}\propto E$ for $P(0)$ finite]. This behavior is in contrast to that in a magnetic field with a short correlation length, for which there is a peak in the density of states near the bottom of the spectrum.[4]

To discuss the density of states at still lower energies, it is necessary to consider wave functions near saddle points of the magnetic field. In the extreme low-energy limit, one should consider rare occurrences of large patches of low magnetic field. Thus one expects strongly localized Lifshitz tail states in the low-energy limit. This regime has been studied by other authors,[4,20] and we do not discuss it further.

In the remainder of this paper we shall be concerned with the nature of eigenstates in the energy range (8), in which states are either weakly localized or extended.

III. THE RANDOM NETWORK MODEL

A. Localization in the semiclassical limit

In this section, we introduce a network model to study localization in a random magnetic field in the semiclassical limit. We follow closely the philosophy of previous work on localization in a uniform field and a smooth scalar potential,[11,25–27] which identified extended states at energies for which the semiclassical trajectories percolate.

Consider first a field distribution which is symmetric about a nonzero mean value $\langle B\rangle$. We argue that cyclotron drift along $B=\langle B\rangle$ contours should percolate through the system and that extended states will be found at energies $E_c(n)=(n+\frac{1}{2})e\hbar\langle B\rangle/m$.[32] Let us focus on the delocalization on a particular eigenenergy surface. Away from the critical energy, the classical guiding-center motion consists of drift along contours closed around hills or valleys of the energy surface, and so the corresponding eigenstates are localized. This geometrical picture, however, omits quantum tunneling. Tunneling is important near saddle points of the random field, at field values close to $B=\langle B\rangle$, and connects disjoint portions of contour at the same field value. The effect of interference between different tunneling paths has been studied in the context of the integer quantum Hall systems, where the semiclassical trajectories reside on equipotentials. Quantum critical behavior, different from that at the classical percolation threshold, is found at the delocalization transition.[33–36] Chalker and Coddington[11] studied this localization transition using a model in which the links of a square network carry quantum-mechanical amplitudes representing the guiding-center drift along an equipotential. Tunneling near saddle points is described by scattering matrices at the nodes of the network. As the critical energy E_c, corresponding to the classical percolation threshold, is approached, the amplitudes for transmission and reflection at saddle points become equal. The localization length diverges as $|E-E_c|^{-\nu}$, with $\nu=2.3\pm0.1$,[37] in agreement with numerical calculations using other models[34] and experimental observations on systems with large Zeeman splitting.[16]

We believe from the arguments sketched above that the same network model is also applicable to semiclassical motion in a random field with finite mean. As proposed in Ref. 5, we expect that, for $\langle B\rangle\neq0$, there is a delocalization transition which belongs to the same universality class as the transition at the center of a spin-split Landau level. This is in agreement with scaling theory,[12,13] which states that the zero-temperature scaling flow is determined by the average Hall conductance of the system.

A different picture, however, arises when the average field is sufficiently small that tunneling between the state on the percolating contour and snake states on a nearby $B=0$ contour is important. In the following, we focus on the case in which the average field is exactly zero, so that the zero-field contours are the ones which percolate. The geometrical properties of the classical snake trajectories on these contours suggest a possible scenario for a delocalization transition in this case of zero average field. At very low energies, there is a Lifshitz tail of states which is certainly localized. These localized states arise because very low-energy particles, traveling along snake trajectories, are reflected at magnetic bottlenecks where the field gradient is large (Fig. 4). At higher energies, there are fewer regions where the field gradient is large enough to create such bottlenecks for the particle. Thus, with increasing energy, the classical trajectories become more extended, and a candidate for a delocalization energy is the corresponding percolation threshold. We will, however, present numerical results showing that, because of quantum interference, even the states arising from these percolating trajectories are localized.

The crossover region, as $\langle B\rangle$ approaches zero, between the zero-mean and finite-mean cases is narrow provided that the correlation length is large. We speculate that, in this region, the extended states levitate in energy with decreasing $\langle B\rangle$, as is believed to happen in quantum Hall systems on decreasing the uniform field.[38–41]

We model the system with zero average field at or above the percolation threshold for the $B=0$ contours as

a random network in which the links represent snake states on these contours. As demonstrated in Sec. II A, these states generically occur in pairs so that, in contrast to the model for a single Landau level, each link of the network model should carry an *even* number of channels. For our numerical work, we choose to stay close to the percolation threshold and study the double-channel network. Networks with more channels per link will have larger conductances at short distances, making it more difficult to reach the asymptotic scaling behavior.

It should be noted that, although finite-B contours are closed, some of the state corresponding to cyclotron drift on these contours will hybridize with the snake states because of reflections at magnetic bottlenecks, as described in Sec. II A and Fig. 4. However, we expect that this affects only the local topology of the resulting percolating network and has no influence on the *universal* aspects of the localization phenomenon that we study.[42] This belief is supported by previous experience with the single-channel version of the model[11] for spin-split Landau levels—the critical behavior extracted from the network model is the same as that obtained[33–36] for a disordered potential projected onto the lowest Landau level.

Considered as a model for motion in a random scalar potential, the nodes of the network allow tunneling near saddle points of the potential. Similarly, the nodes in the double-channel network allow scattering between snake states near saddle points of the magnetic field, where the percolating zero-field contours approach and possibly intersect each other. We discuss next the classical dynamics near these saddle points, and demonstrate that it is chaotic.

B. Classical scattering at the zero-field saddle points

Let us consider classical motion near individual saddle points in the magnetic-field strength, using the field configuration (1) with $b(x/\lambda)=x/\lambda$. We argue that the adiabatic picture breaks down as the classical trajectory crosses the saddle point, and that the subsequent motion is highly irregular.

The approach to the saddle point is simple in the classical adiabatic limit. Consider a snake trajectory approaching the saddle point along the positive-x axis. We show in the Appendix that the trajectory cuts the x axis at angles which are successively closer and closer to $\theta=0$ as the particle approaches the saddle point at $x=0$. Although the adiabatic approximation [that the magnetic gradient changes little on the oscillatory timescale proportional to $(\epsilon/b)^{1/2}$] fails as the gradient b goes to zero, it can be shown that the approach to the origin is collimated. Thus, the particle eventually crosses the y axis within a small region of radius $O(\epsilon^{5/12}\lambda)$, traveling at an angle to the x axis of $O(\epsilon^{1/12})$.

The subsequent motion of the particle, however, is complex and unpredictable. In the neighborhood of the saddle point, the snake trajectories along the x axis are directed toward the origin, while those along the y axis are directed away from it. Suppose that a particle arrives at the saddle point from the negative-x axis. The typical motion is as follows. After the particle has crossed into the region $x>0$, initially traveling nearly parallel to the x axis, it is reflected back toward the origin. It then follows a snake trajectory along the y axis, and away from the saddle point. However, a complete exit from the saddle point is not assured even at this point. The particle may find itself on a trajectory (of low longitudinal velocity) which is easily reflected at a magnetic bottleneck where the magnetic-field gradient is large. Indeed, repeated reflections back toward the saddle point may occur before the particle eventually leaves the saddle-point region. This, in effect, randomizes the final motion with respect to the initial conditions.

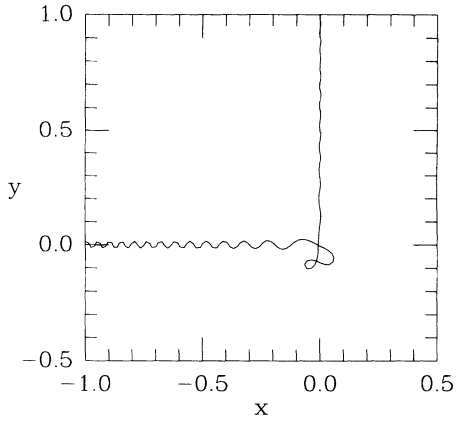

FIG. 5. Simple trajectory. $\epsilon=10^{-4}$. Distance is plotted in units of λ.

We have examined numerically the classical trajectories at an isolated saddle point with field strength given by $B(x,y)=B_0\tanh(x/\lambda)\tanh(y/\lambda)$. We start a particle at a point on the negative-x axis with an initial velocity at an initial angle θ_{in} to the axis. Both simple trajectories (Fig. 5) and chaotic trajectories (Fig. 6) with repeated reflections are found.

Our analysis suggests that scattering at the saddle point destroys any information about the initial conditions of a trajectory. Both the exit direction $\Phi_{\text{out}}=\tan^{-1}(y/x)$ and the exit angle θ_{out} have irregular

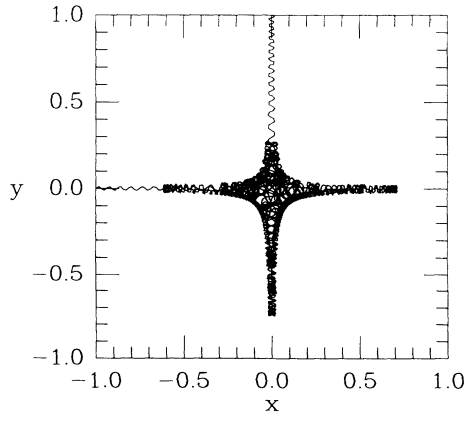

FIG. 6. Chaotic trajectory. $\epsilon=10^{-4}$. Distance is plotted in units of λ.

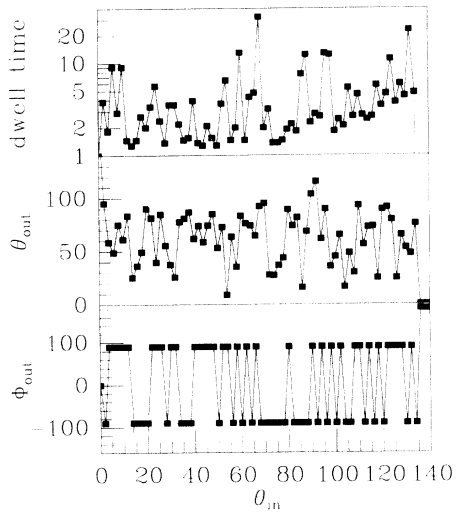

FIG. 7. Exit data for incoming particles with a given θ_{in}. The data for outgoing direction $\Phi_{out}=\tan^{-1}(y/x)$, and exit angle θ_{out} are given for one particular initial position. The dwell time, measured in units of the time taken to traverse the (unstable) straight trajectory along the x axis, is averaged over initial positions. $\epsilon=10^{-5}$.

fluctuations for small changes in the initial angle θ_{in} (Fig. 7). They also change unpredictably for small changes in the initial position. As an illustration of the repeated crossings of the saddle point, we present the dwell time of a particle in a region of radius 3λ around the origin, averaging over initial positions (Fig. 7). One can see that there are indeed trajectories which spend a long time in the saddle-point region in the scattering process. We also present, in Fig. 8, the distribution of θ_{out} for an ensemble of incoming particles with a uniform distribution of θ_{in}. This shows that the distribution of outgoing trajectories is wide, covering all snake trajectories, in spite of the collimation effect on the incoming particle.

C. The two-channel network model

The complexity of the classical motion suggests that quantum scattering at the saddle point should also be irregular. Incoming and outgoing snake channels at a given energy E can be labeled by their wave vector and band index, $k_n(E)$, corresponding to $\cos\theta$ in the classical dynamics. The classical results of Sec. III B suggest that scattering at the saddle point randomizes the band index. This leads us to model quantum scattering at a saddle point using a random scattering matrix. The applicability of random matrix ensembles to scattering problems has been studied extensively for quantum billiards. Although nonuniversal low-energy structures are not included in this approach, it is believed that random matrix theory provides a description of universal stochastic properties of quantum chaotic systems.[43,44]

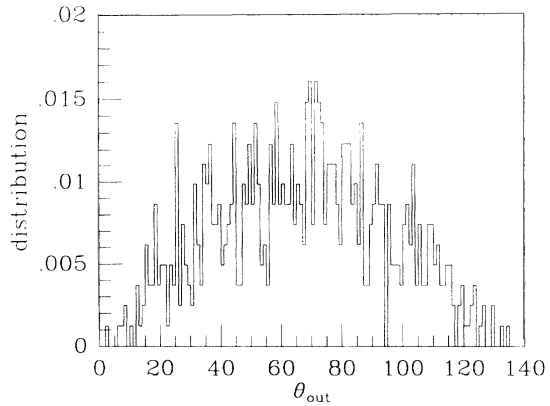

FIG. 8. Histogram of θ_{out} averaged over starting positions and angles. $\epsilon=10^{-5}$.

We begin by recalling the form of the scattering matrix used in the single-channel network model for a Landau level in a random scalar potential. Each link of this network carries quantum-mechanical flux in a given direction. Let $\psi_{in,L}$ and $\psi_{out,L}$ denote the incoming and outgoing current amplitudes on the left of the saddle point; similarly $\psi_{out,R}$ and $\psi_{in,R}$ denote fluxes on the right of the saddle point. The transfer matrix T relates amplitudes on the left of the saddle point to those on the right:

$$\begin{pmatrix}\psi_{out,R}\\ \psi_{in,R}\end{pmatrix}=\mathsf{T}\begin{pmatrix}\psi_{in,L}\\ \psi_{out,L}\end{pmatrix}. \tag{12}$$

Imposing flux conservation, this matrix can be parametrized as

$$\mathsf{T}=\begin{pmatrix}e^{i\varphi_1}&0\\ 0&e^{i\varphi_2}\end{pmatrix}\begin{pmatrix}\cosh\theta&\sinh\theta\\ \sinh\theta&\cosh\theta\end{pmatrix}\begin{pmatrix}e^{i\varphi_3}&0\\ 0&e^{i\varphi_4}\end{pmatrix}. \tag{13}$$

The scattering is characterized by a single parameter θ, which we call the "node parameter," and by the phase shifts $\varphi_{1,2,3,4}$. The transmission probability is $1/\cosh^2\theta$: there is perfect transmission at $\theta=0$ and perfect reflection for $\theta\to\infty$ (see Fig. 9). More generally, it is useful to note the following duality transformation: if the amplitudes $\psi_{out,R}$ with $\psi_{out,L}$ are exchanged, θ should be replaced by θ', where

$$\sinh\theta'=1/\sinh\theta\ . \tag{14}$$

Thus tunneling is maximal when the scattering is symmetric: $\sinh\theta=\sinh\theta'=1$. In the context of potential disorder, this symmetric point corresponds to the center of the disorder-broadened Landau level, at which the localization length diverges, and the limits of small and large θ correspond to low- and high-energy tails of the Landau level.

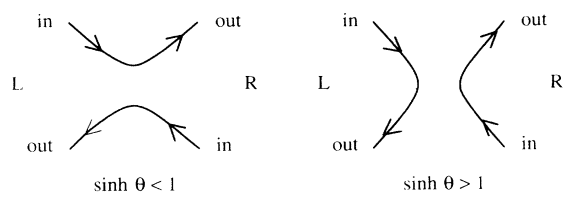

FIG. 9. Transmission and reflection at a node, for different values of the node parameter θ.

In a generalization of this network model, we may have N incoming channels and N outgoing channels on each side of the saddle point, so that $\psi_{\text{in},L}$, $\psi_{\text{out},L}$, $\psi_{\text{in},R}$, and $\psi_{\text{out},R}$ are now N-component spinors. The transfer matrix can be parametrized as

$$\mathsf{T}=\begin{bmatrix}\mathsf{U}_1 & 0\\ 0 & \mathsf{U}_2\end{bmatrix}\begin{bmatrix}\mathsf{C} & \mathsf{S}\\ \mathsf{S} & \mathsf{C}\end{bmatrix}\begin{bmatrix}\mathsf{U}_3 & 0\\ 0 & \mathsf{U}_4\end{bmatrix}, \tag{15}$$

where $\mathsf{U}_{1,2,3,4}$ are $U(N)$ matrices which rotate the individual spinors, and C and S are $N\times N$ diagonal matrices, with diagonal elements $\cosh\theta_i$ and $\sinh\theta_i$ ($i=1,2,\ldots,N$), respectively. This decomposition separates scattering on the network into two contributions. One contribution is represented by $U(N)$ mixing on each link. For $N=2$, it is characterized by phase shifts on the incoming and outgoing amplitudes and also by a mixing angle ϕ:

$$\mathsf{U}=\begin{bmatrix}e^{i\varphi_1} & 0\\ 0 & e^{i\varphi_2}\end{bmatrix}\begin{bmatrix}\cos\phi & -\sin\phi\\ \sin\phi & \cos\phi\end{bmatrix}\begin{bmatrix}e^{i\varphi_3} & 0\\ 0 & e^{i\varphi_4}\end{bmatrix}. \tag{16}$$

The other contribution is represented by the node parameters, and consists of tunneling processes at each node which conserve the channel index i.

The channels in the network model correspond to snake states in our semiclassical limit of electron motion in a random magnetic field with zero mean. As discussed in Sec. III A, the minimum number of channels for this random-field problem is $N=2$ because these snake states generically occur in pairs.

To model disorder, we consider (with some exceptions: see below) the mixers U on each link to be independently and isotropically distributed with the Haar measure. In addition, the node parameters θ_1 and θ_2 must be chosen so that the network has the symmetry of the random-field problem. Taking $\langle B\rangle=0$, the mean Hall conductance of the system should be zero, which requires that the plaquettes of the lattice with clockwise and anticlockwise circulation be statistically equivalent. In the most general case, one can consider the node parameters to be independently distributed, with a distribution which is invariant under the duality transformation (14). In a model of this kind, one expects a crossover from behavior described by classical percolation theory at short distances (due to clusters weakly coupled to the rest of the system), to quantum behavior at long distances. Experience from the single-channel network has indeed shown that fluctuations in the node parameters are irrelevant for the quantum critical behavior.[37,45] For simplicity, we therefore concentrate on networks with identical nodes. Possible networks are then specified by two parameters θ_1 and θ_2. From the condition that the average Hall conductance vanishes, random-field networks lie on the line [as for Eq. (18)]

$$\sinh\theta_1=1/\sinh\theta_2 \quad \text{(random field)}. \tag{17}$$

A schematic illustration of such a network is given in Fig. 10.

Two-channel network models also describe motion in a uniform magnetic field with a random scalar potential, including the spin degree of freedom of the electron. In this case, $U(2)$ mixing arises from spin-orbit scattering.

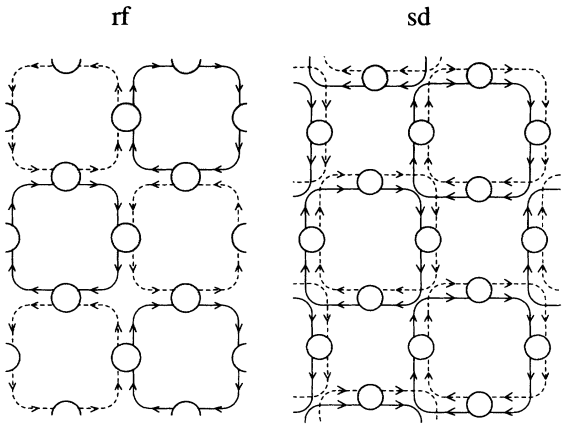

FIG. 10. Schematic illustrations of a random-field (rf) network and a network representing a spin-degenerate (sd) Landau level. The two channels are denoted by full and dashed lines. $U(2)$ mixers are represented by shaded discs.

In particular, the *spin-degenerate* system, in which there is no Zeeman splitting, is represented by networks with

$$\theta_1=\theta_2\equiv\theta \quad \text{(spin-degenerate Landau level)}, \tag{18}$$

so that electrons in both spin states have the same tunneling rate through the saddle points (see Fig. 10). On sweeping the Fermi energy through the Landau level, the system follows line (18) in the (θ_1,θ_2) parameter space from $\theta=0$ to $\theta=\infty$. With Zeeman splitting, this line is displaced so that the two spin states have different tunneling rates at a saddle point: schematically, one can take $\theta_1=(1+g)\theta$ and $\theta_2=(1-g)\theta$, where g represents the electron g factor, with $|g|<1$.

We see that the random-field line (17) and the spin-degenerate line (18) share a common point on this phase diagram, namely the symmetric point: $\sinh\theta_1=\sinh\theta_2=1$. Therefore, conclusions about the behavior of one of these systems carry implications about the behavior of the other.

IV. LOCALIZATION IN THE NETWORK MODEL

A. Phase diagrams

We have arrived at a network model which represents, on different lines in its parameter space, electron motion either in a random magnetic field or in a spin-degenerate Landau level. We now discuss the phase diagram for localization in the full parameter space of this unifying model.

In the absence of scattering between channels, the model would consist of two uncoupled networks, each as studied in Ref. 11. States are localized, except (in the respective networks) on the lines $\sinh\theta_1=1$ and $\sinh\theta_2=1$. In this paper, we are concerned with the consequences of coupling the two networks. We summarize first the implications of the conventional scaling flow diagram proposed by Khmelnitskii[12] for the integer quantum Hall effect. Following Khmelnitskii,[46] let us consider sweeping the Fermi energy through a spin-degenerate

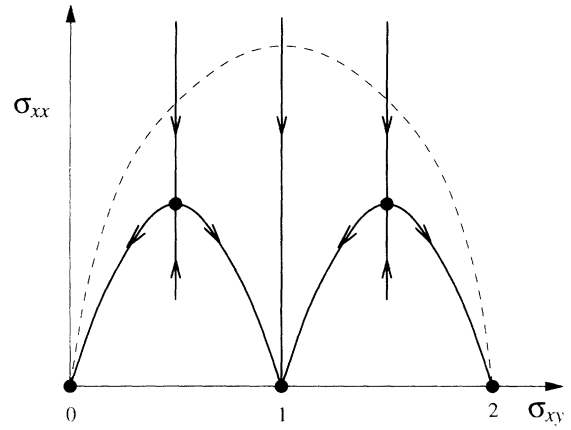

FIG. 11. Khmelnitskii's scaling flow diagram for the integer quantum Hall effect. Fixed points of the scaling flow are denoted by ●. The dashed line indicates the trajectory followed by the bare conductance on sweeping the Fermi energy through a spin-degenerate Landau level, which is the short-distance behavior of the $\theta_1=\theta_2=\theta$ network for $0<\theta<\infty$. σ_{xx} and σ_{xy} are measured in units of e^2/h.

Landau level, traversing the line $\theta_1=\theta_2\equiv\theta$. Along this line, the Hall conductance σ_{xy}, measured at short distances in units of e^2/h, must vary smoothly between $\sigma_{xy}=0$ at $\theta=0$ and $\sigma_{xy}=2$ as $\theta\rightarrow\infty$, following the trajectory indicated by the dashed line in Fig. 11. In particular, at the center of the spin-degenerate Landau level, $\sinh\theta_1=\sinh\theta_2=1$, the Hall conductance has the value $\sigma_{xy}=1$ and scaling flow is toward a localization fixed point. Additionally, there are two isolated points on either side of the Landau-level center, at which $\sigma_{xy}=\frac{1}{2}$ and $\frac{3}{2}$, respectively, and from which the system scales toward delocalization fixed points. Since any trajectory from $\theta_1=\theta_2=0$ to $\theta_1=\theta_2=\infty$ must, on this analysis, share these features, one is led to the phase diagram of Fig. 12(a). In this phase diagram, there are two distinct mobility edges in the spin-degenerate Landau level. Consequently, all states are localized on the line $\sinh\theta_1=1/\sinh\theta_2$ which represents motion in a random field.

In this connection, one point requires further discussion. We have argued that a network representing the random-field problem, with $\sinh\theta_2=\sinh\theta_2=1$, also describes the center of a spin-degenerate Landau level. The equivalence leaves us with the apparently paradoxical requirement that the average Hall conductivity be zero for the former system, but e^2/h for the latter. The paradox is resolved by noting that different boundary conditions apply to the network in the two cases. In a random field, there are no extended current-carrying edge states, while at the center of a spin-degenerate Landau level an edge state contributes one unit to the Hall conductivity. We illustrate this in Fig. 13, comparing the effects of a scalar confining potential on the two systems. Edge states in a random magnetic field carry local currents, in a direction determined by the local sign of the magnetic field, which fluctuates along the boundary. By contrast, in a uniform magnetic field, edge currents flow in the same direction

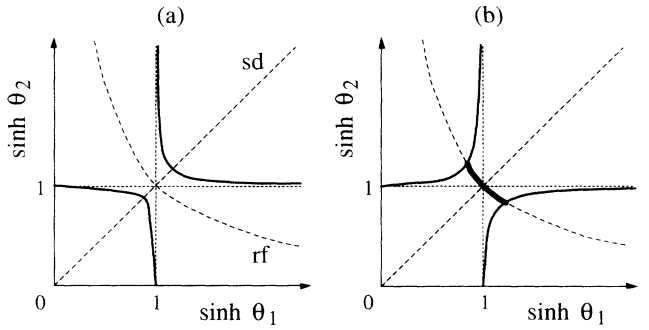

FIG. 12. Schematic phase diagrams. States are extended on the bold lines and localized elsewhere. Dashed lines indicate the parameters of spin-degenerate (sd) and random-field (rf) networks. (a) The phase diagram required by the scaling theory of the integer quantum Hall effect. (b) An alternative.

all along the boundary.

Returning to the phase diagram, we consider only the simplest alternative to Fig. 12(a). It is chosen to accommodate two features: extended states in a random field, as found in some simulations,[3–5] and different critical behavior in spin-split and spin-degenerate Landau levels, as suggested from some experiments.[14–18] In the language of scaling flow for the quantum Hall effect, the latter requires that the two delocalization fixed points in a spin-split Landau level should coalesce if the Zeeman energy is small enough, yielding Fig. 12(b). In this event, states are delocalized only at the *center* of the spin-degenerate Landau level (with, potentially, critical properties in an additional universality class), and there exists a segment of the random-field line along which the localization length is divergent. We argue below that the results of our numerical simulations support the phase diagram of Fig. 12(a).

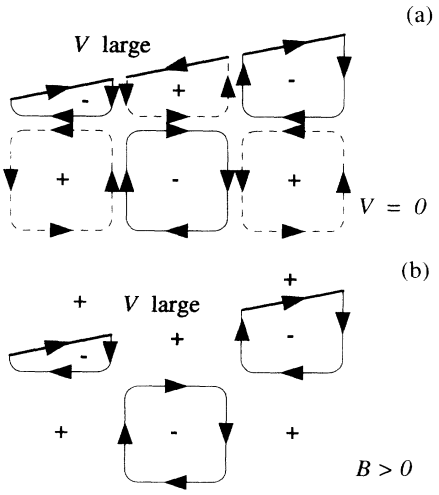

FIG. 13. Edge currents. The edge of the sample is defined as the boundary with a region of high potential V. (a) Random magnetic field: sign of magnetic field denoted by $+/-$. (b) Landau level in a random potential: sign of potential denoted by $+/-$. For clarity, only one of the degenerate spin states is drawn in (b). Edge currents contribute to the Hall conductivity in case (b) only.

B. Numerical results

We use standard numerical transfer-matrix techniques (see Refs. 47–49) to calculate the localization length ξ_M in long samples of the network, of width M, imposing periodic boundary conditions in the transverse direction. We study systems having width $M=8$, 16, 32, 64, and 128, and length 1.2×10^6 links, obtaining ξ_M with statistical errors of less than 1%. We extract the bulk localization length ξ_∞ at each point studied in the phase diagram of the model, using a conventional one-parameter finite-size scaling analysis. This method depends on the assumption that the data from systems of different sizes and at different points in the phase diagram are all described by a scaling function $f(x)$ of one variable, so that $\xi_M/M=f(\xi_\infty/M)$. In fact, it is clear from the scaling flow (Fig. 11) that this cannot be the case everywhere, and that the analysis requires some circumspection. Most obviously, at some points in the phase diagram, systems with large values of ξ_M/M for small M (corresponding to a large bare σ_{xx}) will scale to the delocalization fixed point, while at nearby points, systems which are similar for small M, will scale to localization fixed points. There are two circumstances in which these difficulties are avoided. First, on the random-field line, the value of σ_{xy} does not renormalize and a one-parameter analysis is always appropriate. Second, at sufficiently large scales, all flow comes close to the line joining the delocalization fixed point to the localization fixed point, and a one-parameter description again applies. In practical terms, we require in the second case that ξ_M/M for the widest system studied should be smaller than its value at the delocalization fixed point, $(\xi_M/M)^*\simeq1.2$.[11]

We first present our results for the random-field line, $\sinh\theta_1=1/\sinh\theta_2$. To obtain the full scaling function $f(x)$ from the range of system widths that it is feasible to simulate, we find it necessary to include some generalizations of the model. With random $U(2)$ coupling of the two channels, the localization length remains large, even

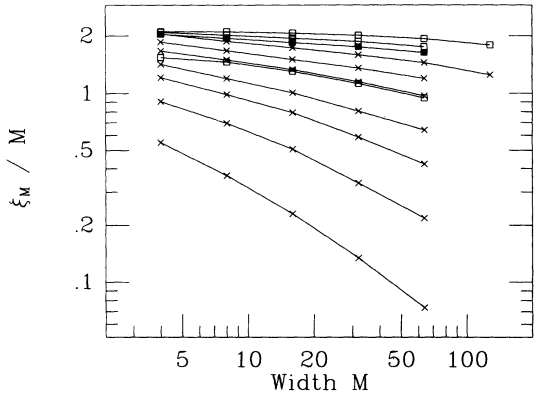

FIG. 14. The localization length in the random-field network as a function of system width. Open squares (□) represent networks on the $\sinh\theta_1=1/\sinh\theta_2$ line with isotropically distributed $U(2)$ mixers ($\sinh\theta_1=1, 1.8, \infty$ from top to bottom); solid squares (■) represent network with random nodes; crosses (×) represent $\sinh\theta_1=1/\sinh\theta_2=0$ networks with fixed ϕ ($0<\phi<\pi/4$).

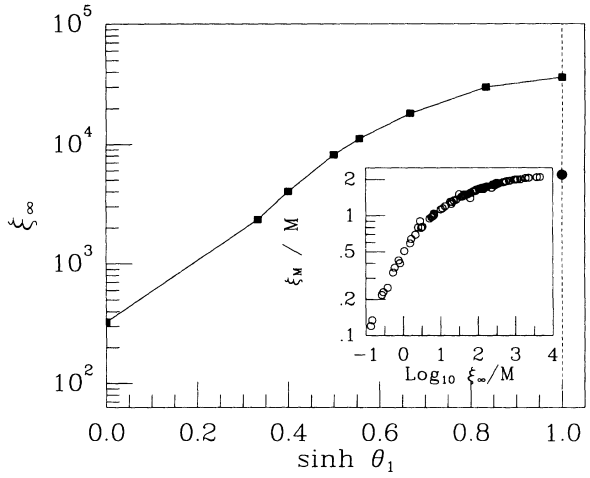

FIG. 15. Bulk localization length ξ_∞ as a function of $\sinh\theta_1$, in the random-field network: squares (■) represent networks on the $\sinh\theta_1=1/\sinh\theta_2$ line with isotropically distributed $U(2)$ mixers; the circle (●) represents a network with random nodes. Inset: one-parameter scaling function $\xi_M/M=f(\xi_\infty/M)$.

in the limit of $\sinh\theta_1\to0$. To obtain the small-x behavior of the scaling function, the regime scaling toward localization, we have therefore also studied a range of networks with $\sinh\theta_1=0$, $\sinh\theta_2\to\infty$, and fixed mixing angle ($0<\phi<\pi/4$). Our data are presented in Fig. 14. The data shown include a network with random node parameters chosen from a distribution which respects, at each node, the constraint that θ_1 and θ_2 are symmetric under the duality relation (14).

The bulk localization lengths which we obtain remain finite everywhere on the line $\sinh\theta_1=1/\sinh\theta_2$. They are displayed in Fig. 15. The largest localization length (of the order of 10^4 lattice spacings) is found for the network with totally symmetric scattering: $\sinh\theta_1=\theta_2=1$. Our results thus select the phase diagram of Fig. 12(a) in preference to that of Fig. 12(b).

We consider next the spin-degenerate Landau level described by (18). On this line, over a narrow range on either side of the level center ($\theta_{\text{center}}\simeq0.88$), the bulk local-

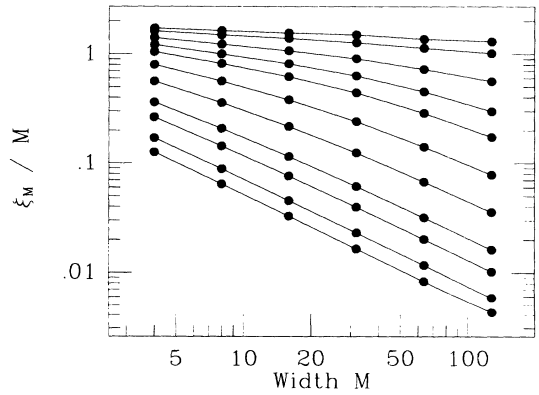

FIG. 16. Localization length in the spin-degenerate Landau level, as a function of system width. Data are presented (from top set to bottom set) for $\theta=1.2$, 1.3, 1.4, 1.5, 1.7, 2, 2.5, 3, 4, and 5.

ization length is so large ($>10^4$) that, with the important exception of its value at the band center (where, as indicated above, the scaling analysis simplifies), we are unable to determine it reliably. We have analyzed data (Fig. 16) for $\theta \geq 1.2$. The divergence in the localization length, as the level center is approached from the band tail ($\theta \gg 1$) is examined in Fig. 17, comparing the two alternative hypotheses represented by Fig. 12. According to the former, one must simultaneously determine the position θ_c of the upper mobility edge, and the value ν of the critical exponent. Since large uncertainties are associated with such a two-parameter fit, we simply demonstrate that there exists a choice of θ_c for which the data are consistent with the exponent value $\nu=2.3$, obtained in previous simulations[11,34–37] of localization in spin-split Landau levels. Moreover, this fit appears better than one taking $\sinh\theta_c=1$. This provides further support for the phase diagram of Fig. 12(a). We suggest that it would be of considerable interest to analyze experiments[14–18] on localization in spin-degenerate Landau levels with the assumption that there are two distinct mobility edges, as in this figure. (This scenario has been discussed in detail by Polyakov and Shklovskii,[50] and also by Wang, Lee, and Wen.[51]) It should be noted that our result is different from the scaling picture of Ref. 18, which allows for a single mobility edge when the Zeeman energy is exactly zero.

Finally, we attempt a precise determination of the critical exponent ν in our model. To do so, we study the line $\sinh\theta_2=2$, which is comparable to introducing Zeeman splitting. In addition, in order to reduce the localization length to measurable values in the range $\sinh\theta_1 \approx 1$, it is necessary to decrease the coupling between channels on each link. We achieve this by abandoning again the isotropic distribution for the $U(2)$ mixing matrices, and restricting the mixing angle to the value $\sin\phi=0.3$. The data are presented in Fig. 18. The localization length diverges as the region $\sinh\theta_1 \approx 1$ is approached from either side. We fit power laws to each divergence, assuming a mobility edge at $\theta_1=\theta_c$, obtaining exponents

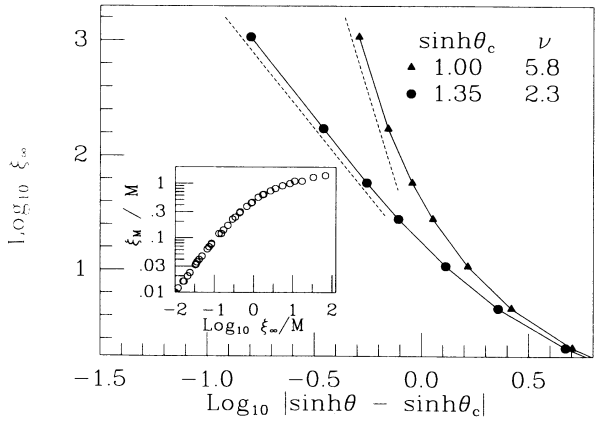

FIG. 17. Divergence of the localization length in a spin-degenerate Landau level. Comparison of fits to the form $\xi_\infty \sim |\sinh\theta - \sinh\theta_c|^{-\nu}$, with a single mobility edge ($\sinh\theta_c=1.00$, $\nu=5.8$) and with two mobility edges ($\sinh\theta_c=1.35$, $\nu=2.3$). Inset: one-parameter scaling function.

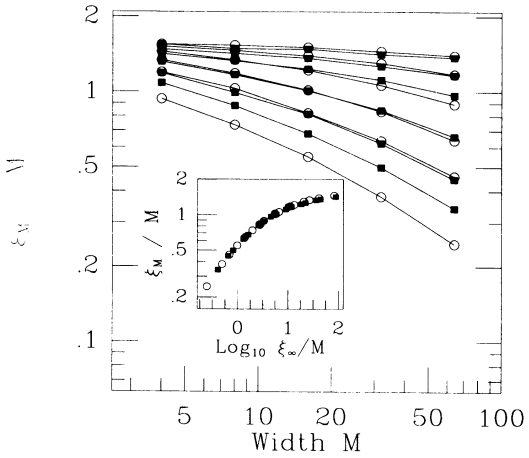

FIG. 18. Network at $\sinh\theta_2=2$. Localization length as a function of system width, on either side of the delocalization transition. Open circles (○) represent data for $\sinh\theta_1<1$: $\sinh\theta_1=0.9$, 0.8, 0.7, 0.6, 0.5, and 0.25 (from top set to bottom set). Solid squares (■) represent data for $\sinh\theta_1>1$: $\sinh\theta_1=1.1$, 1.2, 1.3, 1.5, 1.75, and 2 (from top to bottom). Inset: one-parameter scaling function.

$\nu_-(\theta_c)$ and $\nu_+(\theta_c)$ on each side. Solving the equation $\nu=\nu_-(\theta_c)=\nu_+(\theta_c)$, we obtain $\nu=2.45$ and $\sinh\theta_c=1.00$ (see Fig. 19). This exponent value is remarkably close to the most precise determination for spin-split Landau levels, $\nu=2.34\pm0.04$.[34]

V. SUMMARY

In summary, we have carried out a numerical study of a random network model representing both spin-degenerate quantum Hall systems and localization in a random magnetic field. We conclude that in the model representing motion in a random-field problem there are no extended states. This network model provides a useful description of electron motion in a random magnetic field, which is complementary to the tight-binding model with random flux studied by other authors. Our results are consistent with those of Sugiyama and Nagaosa,[2] but

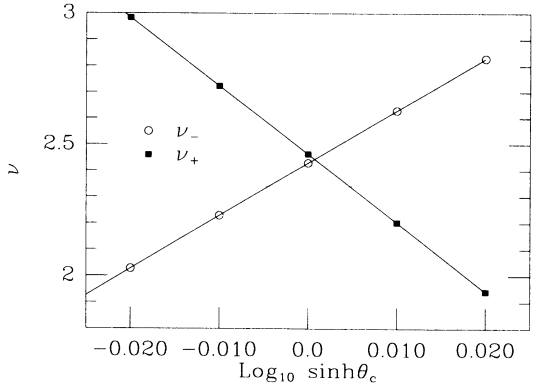

FIG. 19. Network at $\sinh\theta_2=2$. Determination of critical exponent by matching $\nu_+(\theta_c)$ and $\nu_-(\theta_c)$. Horizontal line indicates the value: $\nu=2.34$.

differ from those obtained by other authors[3,5] studying the lattice model, who suggest that there are extended states near the center of the band. We have also established a relationship between localization in a random magnetic field and localization in a spin-degenerate quantum Hall system, by exploiting a semiclassical limit in which the disorder varies smoothly over magnetic length scales and constructing a network model with a parameter space covering both phenomena.

ACKNOWLEDGMENTS

We thank D. Arovas, V. I. Fal'ko, S. M. Girvin, D. E. Khmelnitskii, D.-H. Lee, N. Read, and B. Shklovskii for discussions, and the Aspen Center for Physics for hospitality. This work was supported by the Science and Engineering Research Council (GR/GO 2727) and by the European Community (SCC CT90 0020).

APPENDIX

1. Classical adiabatic theory

We describe here the classical motion of a charged particle along a $B=0$ contour on which the field gradient varies smoothly with position. The equation of motion in the field configuration (1) has been given as Eq. (2). The particle has a snakelike trajectory, cutting the $B=0$ contour at an angle θ (Fig. 1). For $b>0$, it moves in the negative-x direction. It can be easily shown that, for a constant magnetic gradient $\nabla B=bB_0/\lambda$, the amplitude of the lateral oscillations of the snake trajectory is $y_{\max}=2(\epsilon/b)^{1/2}\lambda|\cos(\theta/2)|$. The period of the oscillation is proportional to $(\epsilon/b)^{1/2}$ and diverges as $\theta\to 180°$, and similarly for the longitudinal distance Δx traveled in one period.

The lateral oscillation about the $B=0$ line provides us with an adiabatic invariant:

$$I=\oint m\dot{y}\,dy = 2mv_0\lambda\left[\frac{\epsilon}{b}\right]^{1/2}\sin^2\tfrac{1}{2}\theta \times\int_0^{2\pi}\cos^2 w(1-\sin^2\tfrac{1}{2}\theta\cos^2 w)^{1/2}dw\ . \tag{A1}$$

The action I is an approximate invariant of the motion when the field gradient changes only over length scales much greater than Δx. Within a segment of the contour which is long compared to Δx but short on the scale of the correlation length, one can still identify an angle θ which specifies the motion of the particle. The evolution of θ between segments of different field gradients b is determined by the requirement that I remains constant. From Eq. (A1), one sees that this angle $\theta(x)$ increases, and the drift velocity ($\propto\cos\theta$) decreases, as the particle moves toward a region with a high magnetic gradient. In fact, I has a maximum at $\theta=\theta_0\simeq 135°$ corresponding to a figure-of-eight orbit with zero drift velocity. This means that the particle cannot travel indefinitely into regions of higher and higher magnetic gradients. Instead, it will be reflected at the turning point x_0 given by $\theta(x_0)=\theta_0$. The trajectory of such a particle will eventually join with a finite-B contour (see Fig. 4). Thus a region of large gradient behaves like a "magnetic bottleneck" for particles traveling on $B=0$ contours.

Consider next the situation when the particle approaches a saddle point in the magnetic field at the origin, $b(x/\lambda)=x/\lambda$, from the positive-x axis. For convenience, let us take the unit of length to be λ and the unit of time to be λ/v_0. As the field gradient $b(x)$ decreases, the angle θ becomes small so that

$$I/mv_0\lambda\simeq 2\pi(\epsilon/b)^{1/2}\sin^2\tfrac{1}{2}\theta\ , \tag{A2}$$

and $\sin^4\frac{1}{2}\theta\propto b(x)$ as $b\to 0$. Note that the adiabatic theory breaks down when $b\sim o(\epsilon)$, because Δx then exceeds the correlation length λ. Nevertheless, one can continue to follow the motion of the particle since the equation of motion can be approximated by Stokes' equation when $dx/dt\simeq -1$:

$$\frac{d^2y}{dx^2}=-\frac{1}{\epsilon}xy\ . \tag{A3}$$

The trajectory near the origin is therefore described by Airy functions, $\mathrm{Ai}(z)$ and $\mathrm{Bi}(z)$. One can match the adiabatic theory to the Airy-function trajectories in a common domain of validity: $x\sim\epsilon^{\gamma}$ with $0<\gamma<1$. For $z=x\epsilon^{-1/3}\gg+1$, the shape of the snake trajectory has the asymptotic form

$$y(z)=a[\cos\phi\,\mathrm{Ai}(z)+\sin\phi\,\mathrm{Bi}(z)] \sim\frac{a}{\pi^{1/2}z^{1/4}}\sin\left[\tfrac{2}{3}z^{3/2}+\phi+\frac{\pi}{4}\right]\ , \tag{A4}$$

where a and ϕ are constants determined by initial conditions. By matching the angle of incidence θ given by the adiabatic theory (A2) and by the Airy form (A4) (at the point $x_1=\epsilon^{1/6}$, say), one obtains $a=4\pi\epsilon^{5/6}b_\infty^{-1/2}\sin^2\frac{1}{2}\theta_\infty$, where θ_∞ and b_∞ are initial values of the trajectory at some point x_∞ far from the origin. Substitution into the first line of (A4) gives

$$y(0)\sim\epsilon^{5/12}\ ,\quad y'(0)\sim\epsilon^{1/12}\ . \tag{A5}$$

Therefore, in the adiabatic limit $\epsilon\to 0$, the approach to the saddle point is well controlled. The particle is collimated into a small region around the saddle point, traveling nearly parallel to the x axis.

2. WKB approximation for double-well potential

We summarize here the results, from the WKB approximation, used in the text for quantum motion in a double-well potential described by Eq. (3). Let Λ be the unit of length and E_Λ be the unit of energy. We study only states of positive k in the classically allowed region above the energy barrier $\frac{1}{2}(k\Lambda)^2$. Using rescaled variables $u=y/(8E)^{1/4}$ and $\alpha=k/(2E)^{1/2}$, the Schrödinger equation becomes

$$\left[-\frac{1}{2(2E)^{3/2}}\frac{d^2}{du^2}+(\alpha-u^2)^2-1\right]\psi=0\ . \tag{A6}$$

The quantization condition on the action I is

$$(n+\tfrac{1}{2})\pi = I(E,k) \equiv (2E)^{3/4}\int_0^{(1+\alpha)^{1/2}} \sqrt{2[1-\alpha-u^2)^2]}\,du \ . \quad \text{(A7)}$$

This WKB scheme is valid when the energy of the particle is high enough that the double-well potential is smooth on the scale of the particle wavelength. For Eq. (A6), this means that $2^{5/3}E \gg (1-\alpha^2)^{-1}$, or, in terms of dimensionful quantities,

$$E/E_\Lambda \gg \tfrac{1}{2}(k\Lambda)^2 \ . \quad \text{(A8)}$$

We see that this approximation complements the local-Landau-level regime, in which the particle does not tunnel between the two sides of the double well.

From the quantization condition (A7), one can estimate the turning point in the spectrum $E_n(k)$. The turning point where dE/dk vanishes is given by $(\partial I(E,k)/\partial k)_E = 0$. We find that the minimum for band n occurs at an energy $E_{\min}$ and a wave vector $k_{\min}$ such that

$$E_{\min}(n)/E_\Lambda \simeq \tfrac{1}{2}(k_{\min}\Lambda/\alpha_0)^2 \simeq \tfrac{1}{2}[A(n+\tfrac{1}{2})\pi]^{4/3} \ , \quad \text{(A9)}$$

where α_0 is determined numerically to have the value $\alpha_0 \simeq 0.65$, and $1/A$ is the integral in Eq. (A7) evaluated at $\alpha = \alpha_0$.

One can also estimate the curvature at the bottom of each band in the WKB approximation. This is needed for estimating the singular contribution from this part of the spectrum to the density of states. We find

$$\left[\frac{d^2E}{dk^2}\right]_{E=E_{\min}} = -\frac{\partial^2 I/\partial k^2}{\partial I/\partial E} = \frac{\sqrt{2}A}{3(1+\alpha_0)}\int_0^{(1+\alpha_0)^{1/2}} \left[\frac{1+\alpha_0-u^2}{1-\alpha_0+u^2}\right]^{1/2}(2-\alpha_0+u^2)\,du \ . \quad \text{(A10)}$$

Note that this is independent of the band index.

[1] C. Pryor and A. Zee, Phys. Rev. B **46**, 3116 (1992).
[2] T. Sugiyama and N. Nagaosa, Phys. Rev. Lett. **70**, 1980 (1993).
[3] Y. Avishai, Y. Hatsugai, and M. Kohmoto, Phys. Rev. B **47**, 9561 (1993).
[4] G. Gavazzi, J. M. Wheatley, and A. J. Schofield, Phys. Rev. B **47**, 15 170 (1993).
[5] V. Kalmeyer, D. Wei, D. P. Arovas, and S. C. Zhang, Phys. Rev. B **48**, 11 095 (1993).
[6] S. C. Zhang and D. P. Arovas, Phys. Rev. Lett. **72**, 1886 (1994).
[7] L. B. Ioffe and A. I. Larkin, Phys. Rev. B **39**, 8988 (1989).
[8] N. Nagaosa and P. A. Lee, Phys. Rev. Lett. **64**, 2450 (1990).
[9] N. Read, B. I. Halperin, and P. A. Lee, Phys. Rev. B **47**, 7312 (1993).
[10] V. Kalmeyer and S. C. Zhang, Phys. Rev. B **46**, 9889 (1992).
[11] J. T. Chalker and P. D. Coddington, J. Phys. C **21**, 2665 (1988).
[12] D. E. Khmel'nitzkii, Pis'ma Zh. Eksp. Teor. Fiz. **38**, 454 (1983) [JETP Lett. **38**, 552 (1983)].
[13] H. Levine, S. B. Libby, and A. M. M. Pruisken, Phys. Rev. Lett. **51**, 1915 (1983).
[14] H. P. Wei, D. C. Tsui, M. A. Paalanen, and A. M. M. Pruisken, Phys. Rev. Lett. **61**, 1294 (1988).
[15] H. P. Wei, S. W. Hwang, D. C. Tsui, and A. M. Pruisken, Surf. Sci. **229**, 34 (1990).
[16] S. Koch, R. J. Haug, K. von Klitzing, and K. Ploog, Phys. Rev. Lett. **67**, 883 (1991).
[17] L. W. Engel, D. Shahar, C. Kurdak, and D. C. Tsui, Phys. Rev. Lett. **71**, 2638 (1993).
[18] S. W. Hwang, H. P. Wei, L. W. Engel, D. C. Tsui, and A. M. M. Pruisken, Phys. Rev. B **48**, 11 416 (1993).
[19] B. L. Altshuler and L. B. Ioffe, Phys. Rev. Lett. **69**, 2979 (1992).
[20] D. V. Khveshchenko and S. V. Meshkov, Phys. Rev. B **47**, 12 051 (1993).
[21] D. K. K. Lee and J. T. Chalker, Phys. Rev. Lett. **72**, 1510 (1994).
[22] J. D. Jackson, *Classical Electrodynamics* (Wiley, New York, 1962), Chap. 12.
[23] T. G. Northrop, *The Adiabatic Motion of Charged Particles* (Interscience, New York, 1963).
[24] S. V. Iordansky, Solid State Commun. **43**, 1 (1982).
[25] R. F. Kazarinov and S. Luryi, Phys. Rev. B **25**, 7626 (1982).
[26] S. Luryi and R. F. Kazarinov, Phys. Rev. B **27**, 1386 (1983).
[27] S. A. Trugman, Phys. Rev. B **27**, 7539 (1983).
[28] B. Shapiro, Phys. Rev. B **33**, 8447 (1986).
[29] J. E. Müller, Phys. Rev. Lett. **68**, 385 (1992).
[30] Snake trajectories, which travel in the negative-x direction, are found between $\theta = 0$ and 135°. (For larger θ, the trajectories resemble figures of 8 drifting in the positive-x direction. More details are found in the Appendix.)
[31] D. B. Chklovskii and P. A. Lee, Phys. Rev. B **48**, 18 060 (1993).
[32] Snake states, with high quantum numbers n, are also found at this energy, but they follow zero-field contours which do not percolate and can be neglected in this context.
[33] H. Aoki and T. Ando, Phys. Rev. Lett. **54**, 831 (1985).
[34] B. Huckestein and B. Kramer, Phys. Rev. Lett. **64**, 1437 (1990).
[35] Y. Huo and R. N. Bhatt, Phys. Rev. Lett. **68**, 1375 (1992).
[36] Y. Huo, R. E. Hetzel, and R. N. Bhatt, Phys. Rev. Lett. **70**, 481 (1993).
[37] D.-H. Lee, Z. Wang, and S. Kivelson, Phys. Rev. Lett. **70**, 4130 (1993).
[38] D. E. Khmelnitskii, Phys. Lett. **106A**, 182 (1984).
[39] R. B. Laughlin, Phys. Rev. Lett. **52**, 2304 (1984).
[40] H. W. Jiang, C. E. Johnson, K. L. Wang, and S. T. Hannahs, Phys. Rev. Lett. **71**, 1439 (1993).
[41] R. J. F. Hughes *et al.* (unpublished).

[42]S. V. Iordanskii and B. A. Musykantskii, Zh. Eksp. Teor. Fiz. **103**, 2116 (1993) [JETP **76**, 1055 (1993)].
[43]R. Blumel and U. Smilansky, Phys. Rev. Lett. **64**, 241 (1990).
[44]C. H. Lewenkopf and H. A. Weidenmuller, Ann. Phys. (N.Y.) **212**, 53 (1991).
[45]J. Eastmond, Ph.D. thesis, University of Oxford, 1992.
[46]D. E. Khmelnitskii, Helv. Phys. Acta **65**, 164 (1992).
[47]A. MacKinnon and B. Kramer, Phys. Rev. Lett. **47**, 1546 (1981).
[48]A. MacKinnon and B. Kramer, Z. Phys. B **53**, 1 (1983).
[49]J. L. Pichard and G. Sarma, J. Phys. C **14**, L127 (1981); **14**, L617 (1981).
[50]D. G. Polyakov and B. I. Shklovskii, Phys. Rev. Lett. **70**, 3796 (1993).
[51]Z. Wang, D. H. Lee, and X. G. Wen, Phys. Rev. Lett. **72**, 2454 (1994).

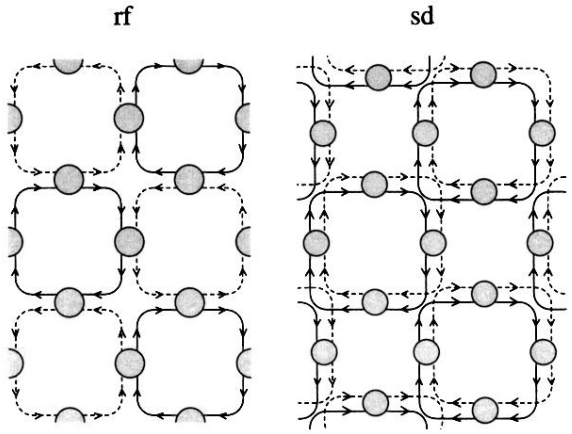

FIG. 10. Schematic illustrations of a random-field (rf) network and a network representing a spin-degenerate (sd) Landau level. The two channels are denoted by full and dashed lines. $U(2)$ mixers are represented by shaded discs.

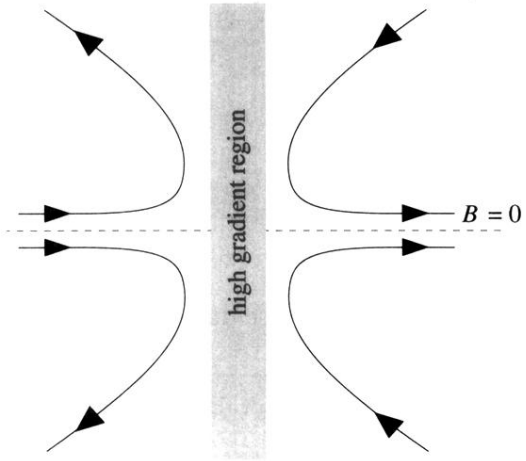

FIG. 4. Schematic illustration of the reflection from snake states onto finite-field contours at a magnetic bottleneck.